Colloids and Surfaces B: Biointerfaces 144 (2016) 21–32

Contents lists available at ScienceDirect

Colloids and Surfaces B: Biointerfaces

journal homepage: www.elsevier.com/locate/colsurfb

Electrospun nanoyarn seeded with myoblasts induced from placental stem cells for the application of stress urinary incontinence sling: An *in vitro* study

Kaile Zhang[a,c,1], Xuran Guo[b,1], Yan Li[c,d,1], Qiang Fu[a,*], Xiumei Mo[b,*], Kyle Nelson[c], Weixin Zhao[c]

[a] *The Department of Urology, Affiliated Sixth People's Hospital, Shanghai Jiaotong University, Shanghai, China*
[b] *Biomaterials and Tissue Engineering Laboratory, College of Chemistry &Chemical Engineering and Biotechnology, Donghua University, Shanghai, China*
[c] *Wake Forest Institute For Regenerative Medicine, Winston-Salem, NC, USA*
[d] *Department Of Gynecology, General Hospital Of Ningxia Medical University, Yinchuan, Ningxia, China*

ARTICLE INFO

Article history:
Received 11 October 2015
Received in revised form 24 March 2016
Accepted 30 March 2016
Available online 1 April 2016

Keywords:
Placental stem cell
Electrospinning
Dynamic liquid electrospinning
Stress urinary incontinence
Tissue engineering

ABSTRACT

Objective: To fabricate a novel electrospun nanoyarn using dynamic liquid electrospinning technique. The nanoyarn will be seeded with myoblasts differentiated from placental stem cells (PSCs) to evaluate the feasiblity of the cell-scaffold construct as a tissue engineering sling to treat stress urinary incontinence.
Material and methods: PSCs were induced to myoblasts with 5-azacytidine and horse serum. Myoblasts differentiation was confirmed by immunofluorescence and western blot. Western blot was also used to assess the change of extracellular matrix (ECM) expression. A dynamic liquid electrospinning system was used to fabricate a novel nanoyarn scaffold for myoblast seeding. Cell morphology and proliferation on nanoyarn and nanofiber scaffold were compared with scanning electron microscopy (SEM) and MTS assay respectively. Filament actin development was tested with Rhodamine-labeled phalloidin stainning; cell infiltration into scaffolds was observed with H&E stainning. ECM expression was evaluated by a collagen assay, immunofluorescence imaging and real-time PCR.
Results: Myoblasts showed increased expression of α-SMA, desmin, and collagen type 1, 3 when compared to PSCs. The nanoyarn possessed higher porosity, larger pore size, and aligned fibers/yarns as compared to nanofiber scaffold. Cell proliferation was significantly improved on nanoyarn scaffold. Cells could infiltrate deeply in the nanoyarn scaffold after 7 days in culture, however, they could only proliferate on the surface of the nanofiber scaffold. The myoblast-nanoyarn constructs seemed to be more like a muscle tissue. The myoblasts spreading on the nanoyarn scaffold were visible with aligned actin filaments in the horizontal view, whereas myoblasts spreading on the nanofiber scaffold were visible with unaligned actin filaments. Nanoyarn myoblasts exhibited higher production and density of type 1, 3 collagen and elastin.
Conclusions: PSCs could be induced into myoblast and expressed elevated myogenic markers and ECM. PSCs are potential cell source for a tissue engineered sling. The novel electrospun nanoyarn scaffold showed potential for use as a sling for treatment of stress urinary incontinence. *In vitro* studies demonstrated that the nanoyarn scaffold could improve cell proliferation, muscular tissue development, and ECM expression compared to random nanofiber scaffolds. The combination of myoblasts and nanoyarn scaffold could be a promising tissue engineered sling for future *in vivo* studies.

1. Introduction

Stress urinary incontinence (SUI) is the most common type of urinary incontinence affecting millions of women worldwide [1]. Sling surgery has become the surgical therapy of choice for stress incontinence in women. In spite of the high success rates,

* Corresponding authors.
E-mail addresses: jamesqfu@aliyun.com (Q. Fu), xmm@dhu.edu.cn (X. Mo).
[1] These authors contributed equally.

http://dx.doi.org/10.1016/j.colsurfb.2016.03.083
0927-7765/

10–20% of women continue to be incontinent. Also, sling erosion, obstructive voiding and persistent pain are possible complications of sling surgery [2]. For patients with persistent urinary incontinence after sling surgery, a tissue engineered sling might be an acceptable option and new trend [3,4].

To date, the application of regenerative medicine for SUI has been predominantly focused on cell therapy in order to restore the natural continence mechanism. It was reported that bone marrow mesenchymal stem cells seeded silk sling showed a doubling of collagen fiber formation with a higher young's modulus as compared to a non-seeded sling, suggesting that the continence mechanism improved [5]. Cell-based therapy and tissue engineering for SUI might be a solution for the future. Previous studies investigating cells for seeding on slings utilized mostly non-induced stem cells or fibroblasts [5,6]. While both stem cells and fibroblasts could produce similar amounts of collagen and increase the leak point pressure (LPP) in an rat model, whereas only stem cell seeding significantly improved urethral muscle strip contractility [6,7]. Furthermore, compared with the high dose stem cell injection therapy, high dose fibroblasts could cause serious urinary retention [6]. These results demonstrated that stem cells could be a suitable cell source for SUI therapy. Embryonic and mesenchymal stem cells have the potency to generate multiple cell lineages, and exhibit self-renewal making them prime candidates for applications in biomedicine [8–10]. Among the great variety of tissues such as bone marrow, adipose tissue and endometrium, the placenta is also a resource to obtain mesenchymal stem cell[11]. Multiple cell types could be differentiated from these cells [12], which provided a candidate of cell source for tissue engineering in urology. Most importantly, the harvesting of placental stem cells does not involve any invasive procedures for the donor and their use does not violate ethics. In previous studies, our group has successfully induced the adipose derived stem cells into myoblasts with 5-azacytidine and horse serum, whether the PSCs could differentiate to the myoblasts with the same protocol is unknown. Furthermore, whether the differentiation of PSC could improve the extracellular matrix (ECM) expression and be used as a cell source for engineered sling is uncertain as well.

In regard to the biomaterials, the traditional electrospinning is a simple and adaptable method for fabrication of scaffolds. The scaffolds fabricated by electrospinning exhibit high porosity and micro- to nano-scale topography, similar to the structure of natural ECM, and are widely used in the engineering of various tissues [13–15]. However, the style of densely packed fibers in the normal electrospun scaffolds is an obstacle for nutrient and waste exchange throughout the scaffolds, which can result in the failure of tissue regeneration [16]. Dynamic liquid electrospinning is a novel technique to make porous scaffold to solve this question. Nanofibers were twisted, rearranged and stacked together to form a micro patterned yarns. The porosity and pore size of the stacked yarns were significantly higher than stacked aligned nanofibers. The main component of human ECM is collagenous fibers. The collagenous fiber is a bundle of collagen fibrils which are formed with twisted procollagen subunits. In the electrospun nanoyarn, the yarns were twisted with a bundle of nanofibers. The topological structure of electrospun yarn is very similar to that of native collagenous fiber. So, compared with other porous scaffold, the advantage of nanoyarn is that the three dimentional structure could biomimic the native collagen fiber.

The nanoyarn was composed of type 1 collagen and P(LLA-CL) (poly(L-lactide-co-caprolactone)), which morphologically and structurally mimics the ECM of native muscle tissue. The nanoyarn scaffolds were seeded with myoblasts induced from PSCs. The morphology and characteristics of the nanoyarn and normal nanofiber scaffold were compared while the muscular tissue development, collagen expression, and cell infiltration of the seeded scaffolds were assessed.

2. Materials and methods

Poly(L-lactide-co-caprolactone) (P(LLA-CL)) (LA:CL = 50:50, Mw = 300,000) was provided by Daigang bioengineering Co. Ltd., Jinan, China. Type 1 collagen was obtained from Ming-Rang Bio-Tech Co. Ltd., Sichuan, China. And 2,2,2-trifluoroethanol was from Fine Chemicals, Shanghai, China.

2.1. Nanoyarn fabrication

A dynamic liquid electrospinning system was used to fabricate the nanoyarn scaffolds (Supplementary Fig. S1). Briefly, a hole (8 mm in diameter) was created in a basin which contained 4–5 l water, so it allowed the flow of water to form a water vortex. A pump was employed to recycle water back to maintain the water level after the water was drained through the hole into a tank below the basin. P(LLA-CL) and collagen was dissolved in HFIP, yielding a 50:50 blended solution (8 w/v%). The blended solution jet located 15 cm above the water vortex, and the spinning rate was 1.0 ml/h under a high voltage of 15 kV. As the HFIP evaporated, electrospun nanofibers were generated and deposited on the water surface; then the nanofibers were twisted into a bundle of nanoyarn in the water vortex and collected by a rotating mandrel (60 r/min) to form a nanoyarn scaffold. After being removed from the mandrel, the nanoyarn scaffold was frozen at −80 °C for 2 h and subsequently freeze-dried overnight. The final nanoyarn scaffold was stored in a vacum oven.

To fabricate a randomly oriented nanofiber scaffold as a control group, the same composition of blended solution as that described for the electrospinning process for nanoyarn was prepared and fed by a syringe. A flat fabric was used to collect the random nanofibers with distance 15 cm from the spinning nozzle.

2.2. Morphology and characterization of nanoyarn and nanofiber scaffolds

2.2.1. Scaffold morphology

The dimension of the whole scaffold was nearly 160 mm × 60 mm × 0.5 mm. The scaffold samples were punched and examined by scanning electron microscopy (SEM). The angle distribution (relative to the vertical axis), diameter, and pore size of the specimens were determined from SEM images using Image J visualization software. The angle distribution and average diameter were measured from 200 random s in the SEM images. The average pore size was determined from 100 pores in a typical SEM image (n = 3).

2.2.2. Scaffold porosity

A vernier caliper was used to measure the exact size and the volumes (V) of scaffold. The scaffold was measured 3 times for the side length and the thickness, an approximate volume could be counted. The dry scaffolds were weighed (Wd), submerged in absolute ethanol (r in density) for 2 h, and weighed again (Ws). The porosity was calculated as (Ws − Wd)/r/V, (n = 3).

2.2.3. Pore size

The pore size of nanoyarn and nanofiber scaffolds was measured with SEM images. Each pore of the nanoyarn and nanofiber scaffold was surrounded and a rhomboid or triangle was formed by yarns, so the length of sides in the triangle and rhomboid was measured and recorded in Microsoft Excel, then the size of the area was calculated

with formula in Excel. The results were defined as the pore size (n = 100).

2.3. Myoblast differentiation

The human placental stem cells were acquired from the institute for regenerative medicine, wake forest university, USA. After passage 5, the PSCs were induced following the previous protocol [17], briefly, the cells were cultured in medium with 10 μl 5-Aza (5-azacytidine, Sigma-Aldrich, USA), 5% (v/v) FBS and 5% (v/v) horse serum (Gibco, USA) and LG-DMEM (Gibco, USA). The differentiation of cells was performed for 2 weeks. Cell growth and morphology were constantly monitored by inverted microscopy. The immunofluorescent staining for the myoblast-specific markers α-SMA and desmin were performed among treated and untreated cells. Rabbit bladder smooth muscle cells (SMCs) and adipose derived stem cells (ADSCs) were used as controls.

2.4. Identification for myogenic differentiation

The success of myogenic differentiation of PSCs and ADSCs were identified with specific biomarkers at day 14. The primary monoclonal antibodies were anti-α-SMA from mouse (Sigma, USA) and anti-desmin from goat (Santa Cruz, USA). After fixation was performed with 4% paraformaldehyde for 10 min. After cells were permeated with 0.2% Triton X-100 for 5 min at room temperature and incubated with the primary antibody for 60 min at 37 °C, the specimens were washed with PBS 3 times and incubated with fluorescent labeled secondary antibody (Donkey anti-Mouse secondary antibody Alexa Fluor® 488 and donkey anti-goat 594) for 30 min at 37 °C. The nucleus were labeled with Fluoroshield Mounting Medium with DAPI. The specimens were examined with a fluorescence microscopy.

2.5. Western blot for muscular markers and collagen

At day 14 of culturing, western blot was performed to measure the relative expression level of collagen type 1, 3 and α-SMA, desmin in PSCs, induced PSCs and SMCs. Lysates of the cell samples were prepared by extracting proteins with the lysis buffer (Ripa and PMSF, Thermal Scientific, USA). Proteins were size-fractionated by sodium dodecyl sulfate polyacrylamide gel electrophoresis and transferred to PVDF membranes (Bio-Rad, USA). The membrane was blocked with Tris-buffered saline with 0.1% Tween-20 (TBST) containing 5% nonfat dry milk at room temperature for 1 h, then it was incubated with primary antibodies from mouse (Abcam, USA) at 4 °C overnight and subsequently with HRP-conjugated goat anti-mouse secondary antibody (Abcam, USA) for 1 h at room temperature. Anti-GAPDH antibody (Abcam, USA) was used as a protein loading control. The results were quantified using Quantity one software (version 4.5.2) and expressed as the ratio of target protein to GAPDH.

2.6. Cell morphologies on scaffolds

The scaffolds were punched into dishes of 12 mm in diameter. Then they were sterilized with ultraviolet for 2 h and put in 24-well plates. 10 Thousand cells in 1 ml complete medium were seeded onto the scaffolds. At day 1, 4 and 7, samples of scaffolds were washed with PBS to remove the non-adherent cells. Then the cells with scaffolds were fixed in 2.5% glutaraldehyde for 30 min at room temperature. Afterwards, they were dehydrated through a series of graded alcohol solutions. The drying process was conducted with the critical point dryer. The scaffolds were sputter coated with gold-palladium (AuPd), and examined under SEM at 12 kV (Tescan Vega, USA).

2.7. Cell proliferation on scaffold

MTS assay ((3-(4,5-dimethylthiazol-2-yl)-5-(3-carboxymethoxyphenyl)-2-(4-sulfophenyl)-2H-tetrazolium)) was used to quantify the cellular metabolic activity following the instruction of the manufacture (Fisher Scientific, USA). The scaffolds were sterilized as previous description. 20 Thousand cells in 1 ml complete medium were seeded on both scaffolds. At day 1, 4, 7, the original medium in 24-well plates was aspirated and added with 100 μl fresh complete medium and 20 μl MTS solution. Then the plate was incubated for 1 h in 37 °C incubator. Afterwards, the medium was collected from the 24-well plates and transferred to 96-well plates. The relative absorbance was measured at 490 nm in a microplate reader (n = 3). The relative absorbance was compared with the standard curve made by seeding different number of cells on scaffolds previously.

2.8. Contraction of scaffold

The contraction of scaffolds with or without cells was assessed at day 4 and 7. The area of scaffolds was measured relative to area at day 0 from digital photographs using ImageJ software (NIH, USA). Cell-mediated contraction was evaluated by subtracting the difference between scaffolds with and without cells.

2.9. Mechanical property test of scaffolds

At day 7, The cross-sectional area was measured with using a caliper, scaffold samples were cut into 5 mm × 20 mm rectangular samples. The width and thickness of samples were measured with calibrated digital calipers. The length was then measured as the clamp to clamp distance. The mechanical characteristics were tested with an Instron tensile testing machine (Model #5544, Instron Corporation, Norwood, MA, USA) equipped with a 100 N load cell. Tensile strength, Young's modulus and elongation at break tests were conducted with a constant crosshead speed of 2 mm/min until failure.

2.10. H&E staining

Cells seeded scaffolds were paraffin embedded, then hematoxylin-eosin (H&E) staining was used to test the cell infiltration. After 4 and 7 days post-seeding, the cell-seeded scaffolds were rinsed with PBS and fixed in 4% paraformaldehyde for 15 min at room temperature followed with dehydration and paraffin embedding. Afterwards, the specimens were stained with H&E and observed under an optical microscope.

2.11. Rhodamine-labeled phalloidin stainning

After 4 and 7 days, the specimens of myoblasts seeding on nanoyarn and nanofiber scaffold were rinsed twice with PBS (3 min per wash), then the scaffolds were fixed with 4% paraformaldehyde for 10 min. Afterwards, The cells were penetrated using 0.1% Triton X. 5 μl rhodamine-labeled phalloidin (Biotium, USA) in 200 μl PBS was used to stain the cytoskeletons, DAPI (Beyotime, USA) was used to stain the nuclei of the myoblasts on the scaffolds. The stained specimens were observed with laser confocal microscope.

2.12. Collagen production assay

At day 4 and 7, the scaffolds with cells in 24-well culture dishes were rinsed with PBS twice, lysis buffer (Ripa and PMSF, Thermal

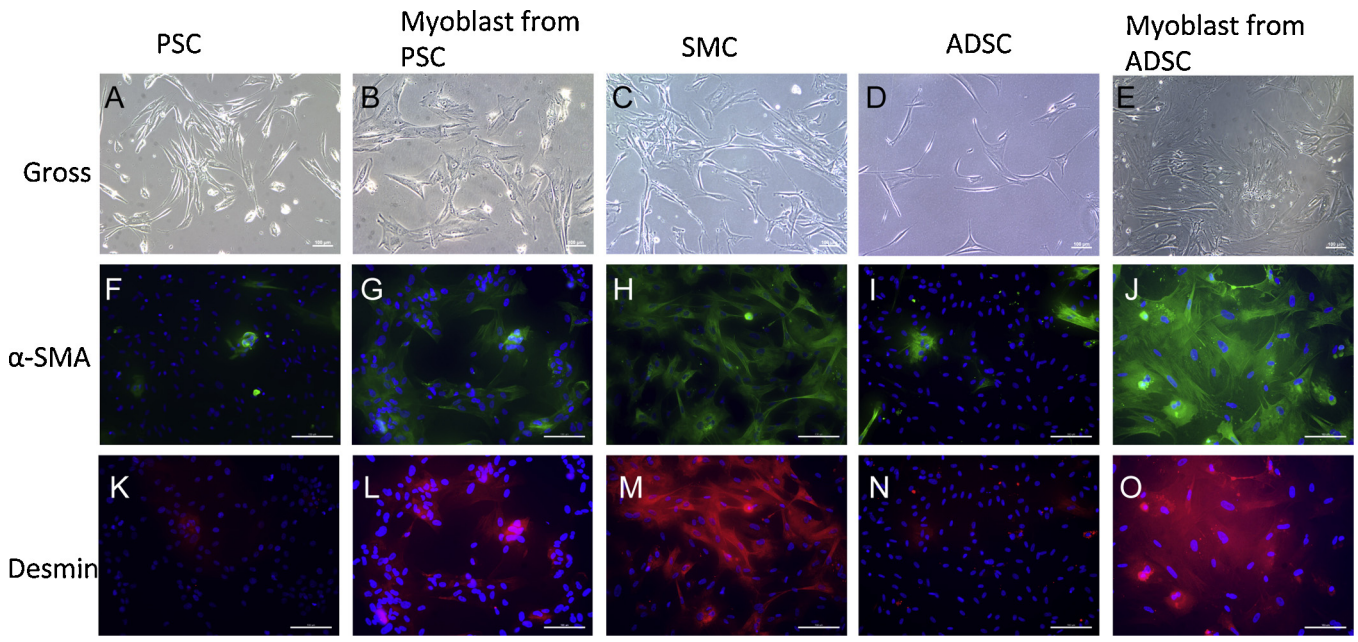

Fig. 1. The microscopy image and immunofluorescence of different cells. PSCs (A, F, K), Differentiated PSC (B, G, L), SMC (C, H, M), ADSC (D, I, N), Differentiated ADSC (E, J, O). α-SMA was immunostained as green, and desmin was immunostained as red, nuclei were stained as blue. Scale bar = 100 μm. (For interpretation of the references to colour in this figure legend, the reader is referred to the web version of this article.)

Scientific, USA) was used to collect the collagen. Then the buffer was tested with the QuickZyme soluble collagen assay kit (QuickZyme Biosciences, USA). The following procedure was conducted with the instruction of the manual.

2.13. Immunofluoresence of extracellular matrix

At day 7, the samples of scaffolds were stained with fluorescence labeled antibodies for detecting ECM. The primary monoclonal antibodies were anti-collagen type 1, anti-collagen type 3 and anti-Elastin from mouse (Sigma, USA). After permeabilization with 0.2% Triton X-100 for 10 min at room temperature and incubation with the primary antibody for 60 min at 37 °C, the specimens were washed with PBS for 3 times and incubated with fluorescent labeled secondary antibody (Donkey anti-Mouse IgG Secondary Antibody, Alexa Fluor® 488 or 594 conjugate) for 30 min at 37 °C. The nuclei were stained with DAPI for 5 min and rinsed 3 times. The specimens were examined with confocal fluorescence microscope. The specimens incubated with secondary antibody but without primary antibody was used as control. The fluorescence density was evaluated with Image J.

2.14. Real-time polymerase chain reaction

The sensing and responding pattern of the myoblasts on nanofiber scaffold and nanoyarn were determined. The specific genes expression (Type 1 collagen, type 3 collagen, a-SMA and desmin) were analyzed with real-time polymerase chain reaction (PCR) at day 7 after culturing. The myoblasts in 10 cm culture dish were served as controls. β-Actin was used as housekeeping gene. Total RNA was extracted form myoblasts cultured on different scaffolds with Rneasy Mini kit (QIAGEN, USA). The RNA was transcribed reversely to cDNA with a high capacity cDNA synthesis kit (Lifetechnologogies, USA). Real-time PCR was performed with PCR master Mix on a light cycle apparatus. All the gene expression probes were acquired from the TaqMan® Gene Expression Assays (Lifetechnologies, USA). Three replicate analyses were performed for each specimen, and three PCR runs were performed for each gene. The level of relative gene expression was displayed as $2^{-\triangle\triangle Ct}$.

2.15. Statistical analysis

The quantitative data were presented as the mean ± standard deviation. One-way analysis of variance was used to assess the statistical significance of results between each group. Difference was considered significant when $p < 0.05$.

3. Results

3.1. PSCs differentiation

The morphology of adhering PSCs (Fig. 1A) and ADSCs (Fig. 1D) exhibited a fibroblast-like spindle shape. After treated with 5-Aza and horse serum medium, the differentiated PSCs (Fig. 1B) and ADSCs (Fig. 1E) developed to the shape similar to the bladder smooth muscle cells (Fig. 1C) with larger cytoplasm. The expression of α-SMA and desmin could be detected in the PSCs (Fig. 1G,L) and ADSCs after inducing (Fig. 1J,O). As a positive control, the markers were also highly expressed in SMCs (Fig. 1H, M). Low expression of α-SMA and desmin were detected in the untreated PSCs (Fig. 1F,K) and ADSCs (Fig. 1I,N).

3.2. Muscular marker and ECM expression

Fig. 2 showed the Western blot performed at day 14 after inducing for relative quantitative analysis of collagen type 1,3 and α-SMA, desmin. The blots of collagen type 3, α-SMA and desmin were intensified obviously in the image (Fig. 2A). The expression of collagen type 1 elevated but not significantly in myoblasts compared with that in PSCs (Fig. 2B). After inducing, collagen type 3, α-SMA and desmin in myoblasts expression elevated significantly compared with PSCs (Fig. 2B,C).

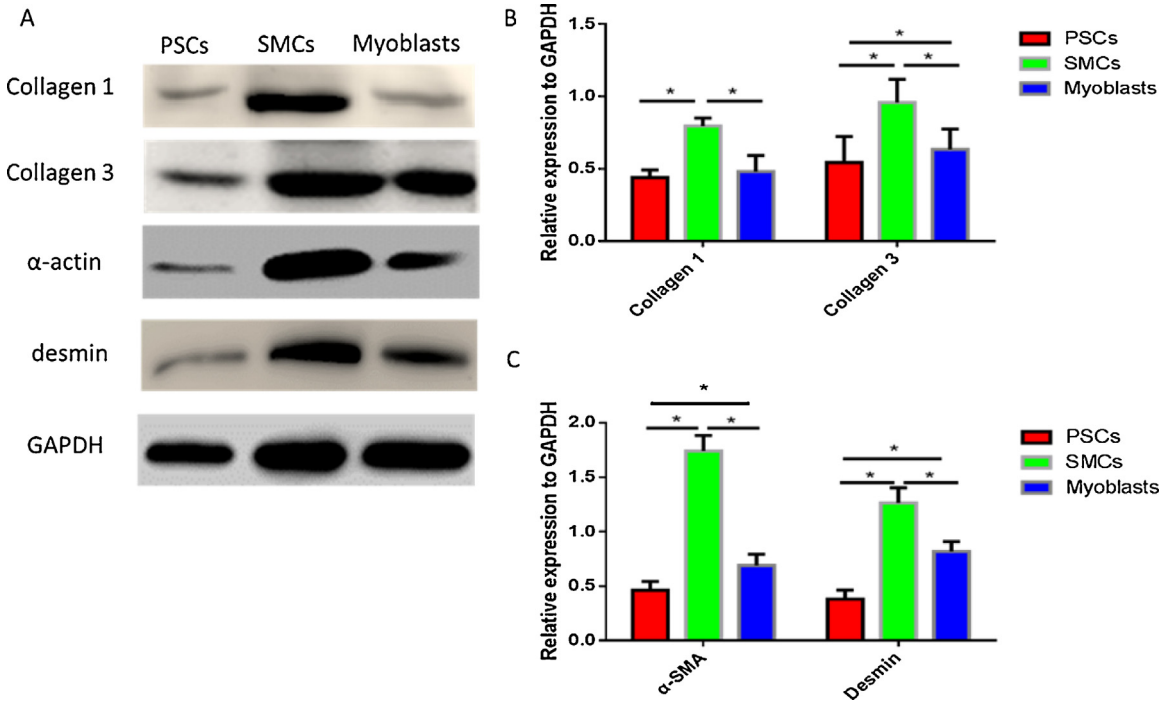

Fig. 2. Western blot analysis. (A) Western blot of collagen type 1, 3, α-actin and desmin produced in PSCs, SMCs and Myoblasts. (B) The quantitative evaluation of collagen type 1 and 3; and (C) The quantitative evaluation of α-SMA and desmin. *$p < 0.05$, $n = 3$.

3.3. The morphology and characteristics of scaffolds

Fig. 3 showed the SEM and quantitative analysis of different scaffolds. The higher magnification images showed that the nanofibers in the nanoyarn scaffold was twisted into yarns (Fig. 3E,F). The images of SEM were analyzed with Image J (NIH, USA). The pore size exhibited in nanoyarn scaffold (32.5 ± 3.32 μm) was larger than nanofiber scaffold (6.24 ± 1.2 μm) significantly (Fig. 3G). The nanoyarn porosity ($85.2 \pm 5.3\%$) increased significantly compared with that in the nanofiber scaffold ($72.3 \pm 9.4\%$) (Fig. 3H). The angle of nanofibers in the nanoyarn mainly ranged from 0° to 20° (Fig. 3J), but the fiber angle of nanofiber scaffolds distributed equally from 0° to 90° (Fig. 3I). The "turns per cm" could be observed in Fig. 3D. The fibers in the yarn turned nearly 180° in 100 μm, thus there is 50 turns in 1 cm yarns.

3.4. Cell morphology and proliferation on scaffolds

Fig. 4 showed the SEM of myoblasts morphology on the scaffolds after 1, 4 and 7 days in culture. Myoblasts were well spreaded on the nanofiber scaffold and exhibited a random orientations at day 1 (Fig. 4A), day 4 (Fig. 4B), and day 7 (Fig. 4C). As shown in Fig. 4G, Myoblasts adhered on both scaffolds with similar number at day 1. Cells proliferated significantly from 1 day to 7 days' culture in both scaffolds. The cell number in nanoyarn is higher than that in the nanofiber scaffold with significant difference ($p < 0.05$).

3.5. Contraction of scaffold

Fig. 5A showed the scaffold contraction rate after 7 days for unseeded and cells seeded scaffold respectively. Digital photographs and Image J software (NIH, USA) were used to calculate the contracted area relative to the initial area at day 0. The cells seeded scaffold had higher contraction rate than the unseeded in both nanofiber scaffold and nanoyarn. The contraction rate of nanofiber scaffold is significantly higher than that of the nanoyarn at day 7.

3.6. Mechanical properties of scaffolds

Fig. 5B–D displayed the mechanical properties of the scaffold samples. The nanoyarn showed lower Young's modulus (Fig. 5D), lower tensile strength (Fig. 5B) but higher elongation at break (Fig. 5C) compared with nanofiber scaffold. After the myoblasts were seeded and cultured for 7 days, the nanoyarn revealed an elevation of tensile strength (Fig. 5B) and Young's modulus (Fig. 5D) significantly. However, the elevation of mechanical properties in nanofiber scaffold was not significant after cell seeding (Fig. 5B–D).

3.7. Cell infiltration

Fig. 6 showed the cell infiltration in the different scaffolds. The nanoyarn (Fig. 6C,D) was found to yield a significantly enhanced cell infiltration compared with nanofiber scaffold (Fig. 6A,B). The depth and distribution of cell infiltration were calculated according to the scale bar in the H&E image. As shown in Fig. 6E, at day 7, the cells infiltrated into the nanoyarn scaffold with approximately 100 μm compared with 5 μm in nanofiber scaffold. At day 14, the depth of cell infiltration in the nanoyarn (approximately 400 μm) was significantly deeper than that in the nanofiber scaffold (5 μm). As shown in Fig. 6F, majority of cells in nanoyarn distributed within 100 μm after 14 days culturing, some cells infiltrated into 600 μm in depth.

3.8. Filament actin staining

The myoblasts on different scaffolds were stained with rhodamine-labeled phalllidin and DAPI (Fig. 7). The myoblasts spreading on the nanoyarn scaffold were visible with aligned actin filaments at day 4 (Fig. 7C) and day 7 (Fig. 7D), whereas myoblasts spreading on the nanofiber scaffold were visible with unaligned actin filaments at day 4 (Fig. 7A) and day 7 (Fig. 7B). At day 7, the morphology of cells were elongated and spreaded evenly on the nanoyarn, aligned actin filaments were observed parallel to the axis

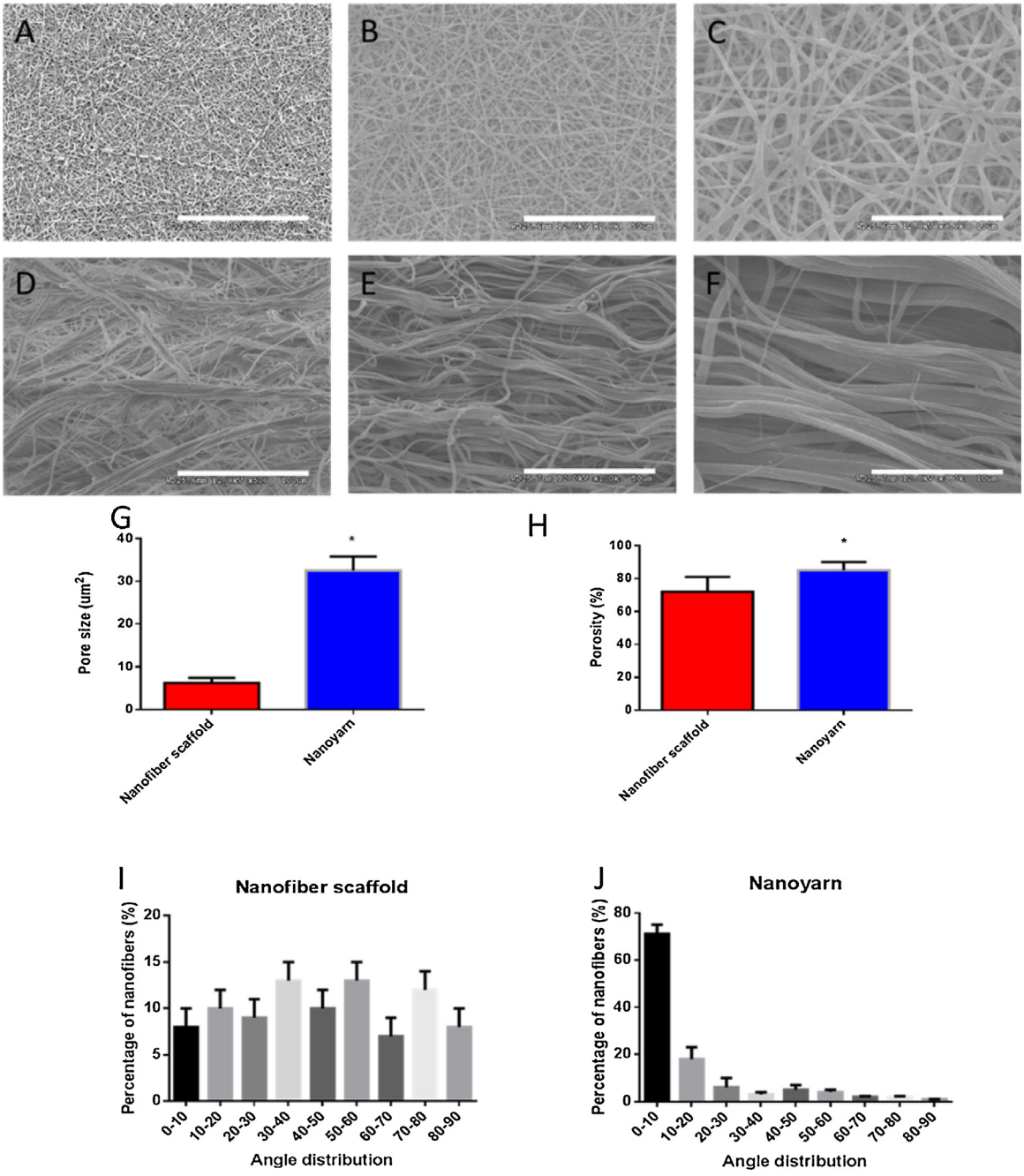

Fig. 3. SEM and characteristics of different scaffolds. Nanofiber scaffold (A, B, C) and nanoyarn scaffold (D, E, F) at different magnification. (G) The pore size; (H) The porosity; the angle distribution of nanofiber scaffold (I) and nanoyarn (K). *$p < 0.05$. The scale bars in figure A, D represented 100 μm, those in figure B, E represented for 50 μm, and those in figure C, F represented for 10 μm.

of the cell elongation, which were much more like the tissue of muscle (Fig. 7D). However, the actin filaments of cells on the nanofiber scaffolds were short and spreaded randomly (Fig. 7B).

3.9. Collagen assay

Supplementary Fig. S2 showed the collagen assay results for collagen in the scaffolds and culture dishes. From day 4 to day 7, the collagen production was increasing in both scaffolds and 24-well dishes (2D culturing). The highest amount of collagen was detected in the nanoyarn scaffolds and was significantly higher than that in nanofiber scaffold and 2D culturing on day 4 and day 7. The collagen in nanofiber scaffold was lower than 2D culturing at day 4 and day 7, but not significantly.

3.10. Immunofluoresence staining

Fig. 8 showed the ECM of Myoblasts with immunofluorescence. The fluorescence was observed with confocal microscopy. The myoblasts on the nanoyarn scaffold showed higher expression of collagen type 1 (Fig. 8F), collagen type 3 (Fig. 8G) and elastin (Fig. 8H) than that on the nanofiber scaffold (Fig. 8B–D). The density of fluorescence was calculated with the Image J. The percentage of fluorescence area was significantly elevated for collagen type 1 (Fig. 8I), collagen type 3 (Fig. 8J) and elastin (Fig. 8K). The control

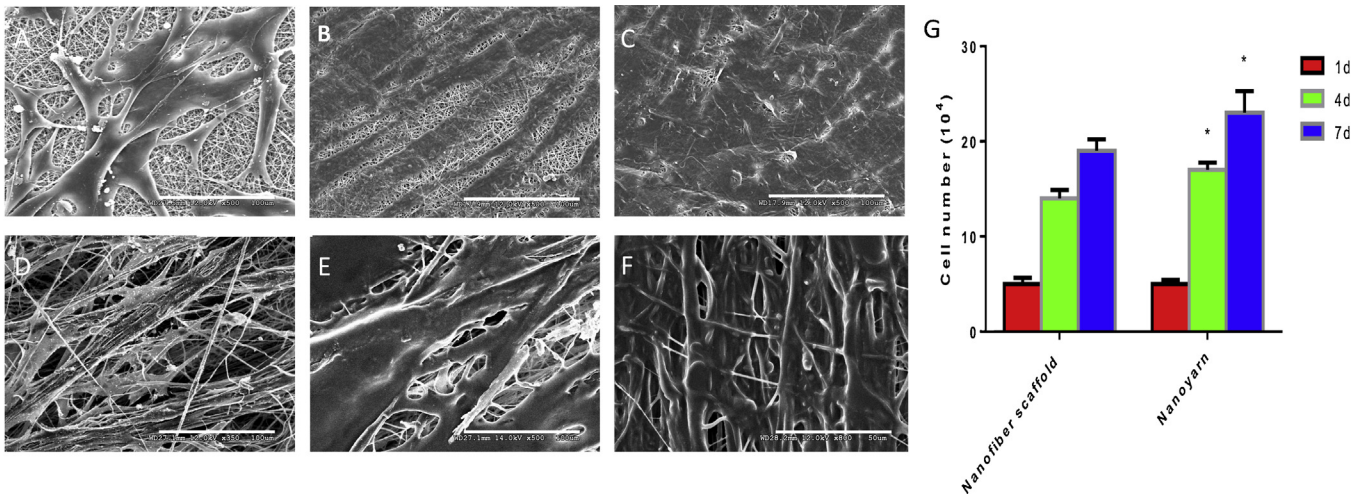

Fig. 4. SEM of myoblasts on nanofiber scaffold and nanoyarn. At day 1, day 4 and day 7 after culture, myoblasts on nanofiber scaffold (A, B, C) and nanoyarn (D, E, F). (G) The proliferation rate of myoblasts on scaffold. *$p < 0.05$ compared with nanofiber scaffolds. The scale bars represents 100 μm in Figure A–E and 50 μm in Figure F.

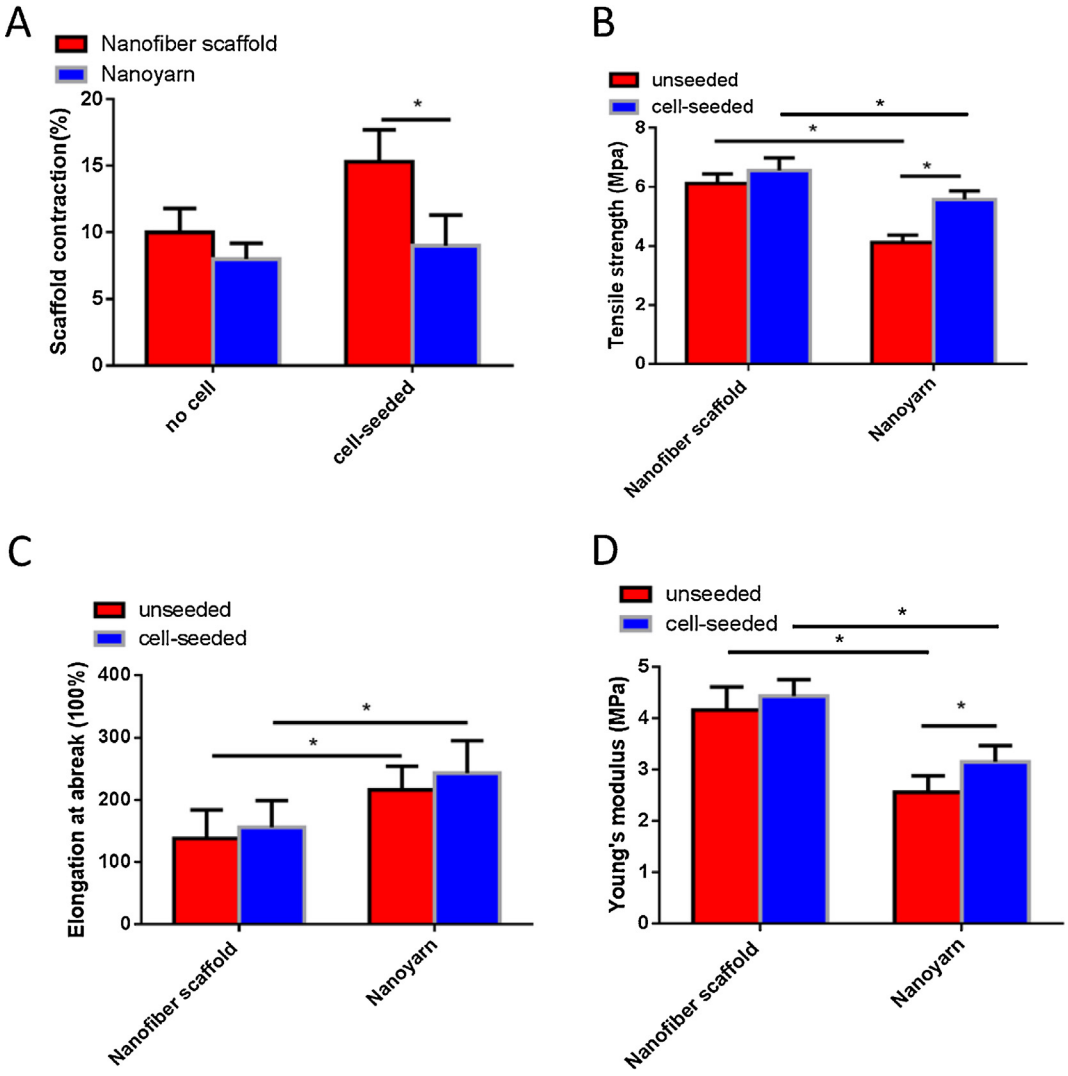

Fig. 5. The contraction rate and mechanical properties of different scaffolds. (A) The contraction rate of scaffolds with or without cells after 7 days culture (n = 5). (B) The tensile strength, (C) Elongation at break, and (D) Young's modulus of the scaffolds. *$P < 0.05$, n = 3.

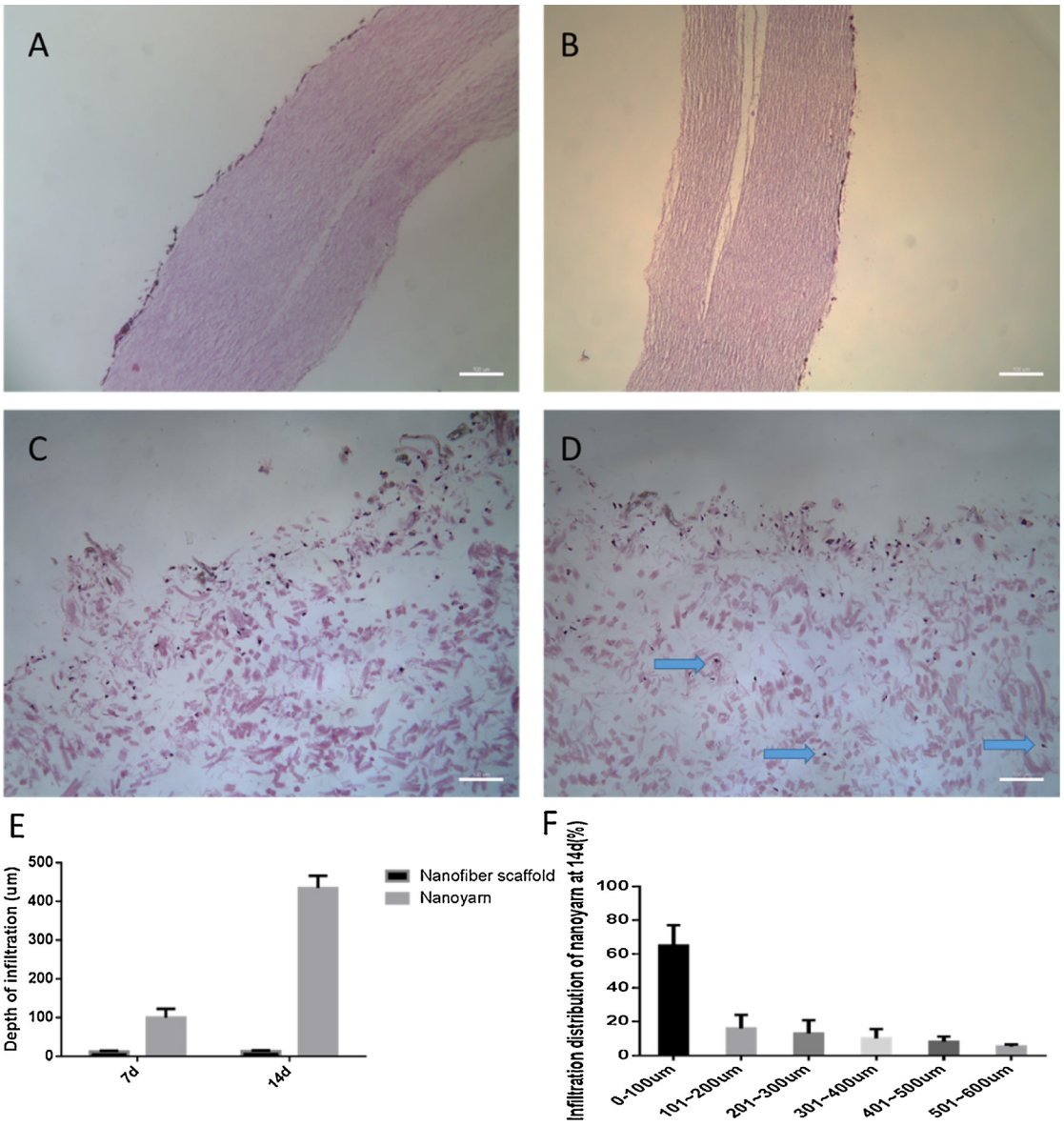

Fig. 6. The infiltration of myoblasts into the scaffolds. Cell seeded nanofiber scaffold at day 4 (A) and day 7 (B); cell seeded nanoyarn at day 4 (C) and day 7 (D). (E) The depth of cells infiltration in different scaffolds, (F) the infiltration distribution of cells in the nanoyarn. The scale bars represented 100 μm in the figures.

group in each scaffolds showed blue fluorescence of DAPI but no obvious green or red fluorescence stained (Fig. 8A,E).

3.11. mRNA expresssion

Supplementary Fig. S3 displayed the mRNA expression of the ECM and muscle related genes expression profiles for myoblasts cultured on the different scaffolds. At day 7, the collagen type 1, collagen type 3, elastin, α-actin and desmin expression elevated significantly on the nanoyarn compared with the nanofiber scaffold.

4. Discussion

SUI is an increasingly prevalent disease. Suburethral sling surgery remains the mainstay of surgical treatment for SUI [18]. Despite the high success rate, synthetic sling surgeries are liable to cause complications [18]. The complications could be recurrence,urinary retention, erosions, extrusions, groin pain, leg pain, bladder perforation, urethral perforation and deep vein thrombosis [19]. Tissue engineering might be a potential option to solve the underlying problem of SUI patients rather a symptom-relief approach. Tissue engineering seeks to use a combination of cells and material to regenerate diseased tissue [7]. Although considerable progress has been obtained in this field, there have been few products available for clinical applications in tissue engineered sling over the past years. One important cause for this scarcity is that the scaffold for sling with desirable properties are still under development, and the choice of cell type is a key question to the success of tissue engineered sling as well.

Regenerative medicine involves the use of cells to repair or replace damaged tissues for the restoration of their normal function. Stem cells are promising candidates for use in tissue engineering and regenerative medicine applications as they possess unique characteristics of self-renewal and differentiation into variety of cell types. Stem cells are present in various adult and neonatal tissues. Mesenchymal stem cells (MSCs) are the primary source of stem cells tested for therapeutic benefit in urologic applications.

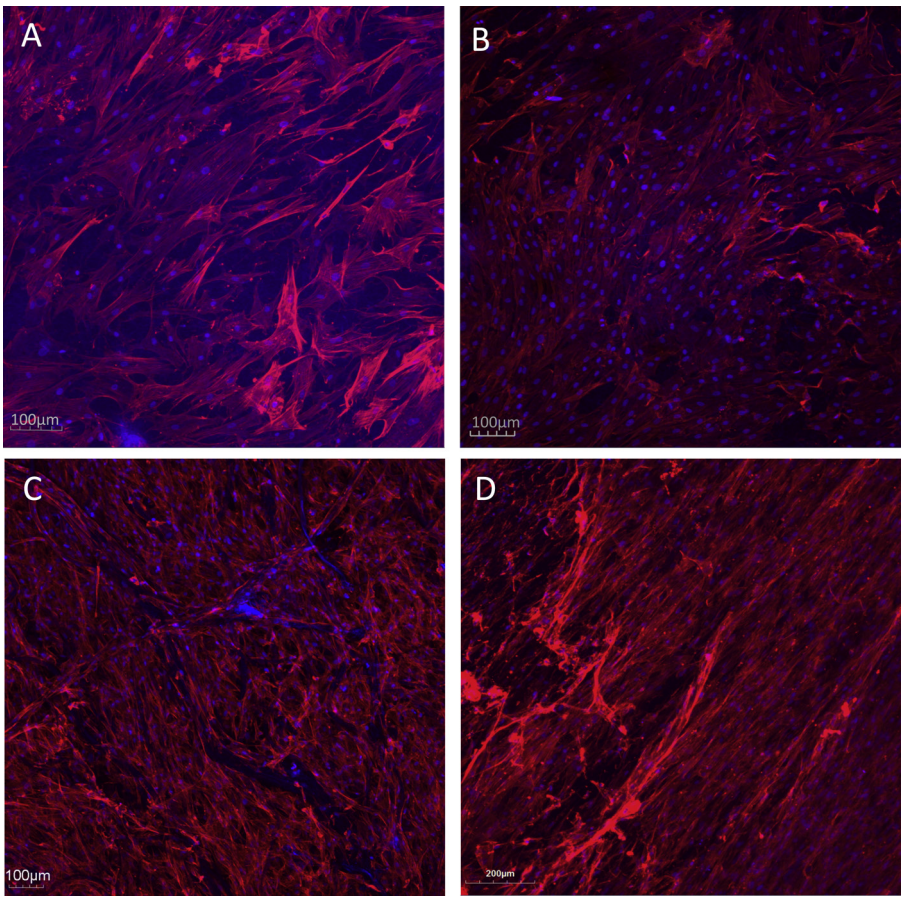

Fig. 7. The confocal microscopy image of filament actin of myoblasts on different scaffolds. Myoblasts on nanofiber scaffold at day 4 (A) and day 7 (B), and nanoyarn at day 4 (C) and day 7 (D).

Whereas, this cell population is relatively rare in bone marrow and traditional bone marrow procurement is painful, requires general or spinal anesthesia, and potentially produces low yield. Recently, PSCs were introduced to the field of tissue engineering. These cells have regenerative and revascularization potential and are low-immunogenic, which is potentially advantageous in hopefully assisting them to become well integrated into host muscle tissues. Secondly, PSCs could be easily and rapidly extracted from perinatal tissue which opens the possibility of clinical application. The PSCs were induced to myoblasts, which showed higher level of muscle cell markers and collagen types 1 and 3 expression (Figs. 1and 3).

Ideal engineered scaffolds should mimic the native ECM to support cell adhesion, proliferation and differentiation biologically and architecturally, thereby facilitating tissue development [16]. Electrospinning is reported to be an efficient and economical process to fabricate scaffolds for tissue engineering applications [20]. Various natural or synthetic polymers have been fabricated into engineered scaffolds with electrospinning method for the repair of many different types of tissues [21–23]. Promising as electrospinning technique is, the fabrication of scaffolds with 3D property remains to be a problem, due to its nature of layer-by-layer deposition of the nanofibers [24]. The densely packed fibers of the scaffolds restricted the nutrient exchange and metabolic product removal throughout the scaffolds, which could result in the incomplete regeneration of the tissue [16]. To solve this problem, the previous methods were salt leaching, ice crystal formation, sacrificial fibers or increasing the fiber diameter Baker et al. [25]. However, these methods would decrease the mechanical property and inhibit the cell growth seriously due to some toxic polymers. Previously, our group introduced a nanofibrous scaffold which was blended with nanoyarns to increase the pore size. This scaffold was fabricated with a rotating device in dry environment. Although more cells infiltrated in the scaffold compared with simple nanofibrous scaffold, but the number is limited due to the hinder of nano-scale fibers [26].

There are several studies demonstrating the positive impact of alignment and large pores of the scaffold to cells [27,28]. In the present study, a P(LLA-CL)/collagen nanoyarn with porous, aligned and 3D microstructure was fabricated with a novel electrospun fiber manipulation process. The characteristics of large pore, high porosity and aligned fibers provided a satisfactory biomimetic environment for myoblasts. These properties could facilitate the cells to form muscle morphologically and structurally.

It was reported that the cells are very sensitive to structure, fiber diameter, and orientation, which could affect the differentiation and function of cells [29]. Our primary goal is to fabricate a porous scaffold to form muscular tissue with 3D structure, secondary goal is to get the alignment to mimic the aligned muscle fiber. The property of alignment is decided by our harvesting process. We found that this property could guide the direction of cells' growth, but could not promote the proliferation and infiltration of cells significantly compared with random nanofiberous scaffold [26]. Some studies found that aligned scaffolds displayed significantly increased expression of tenomodulin compared to nonaligned scaffolds [27]. In the present study, we used the mandrel to collect aligned nanoyarn to guide the cells in one direction to mimic the muscle tissue. Myoblasts seeded on the nanoyarn scaffold presented an elongated morphology in SEM image and also

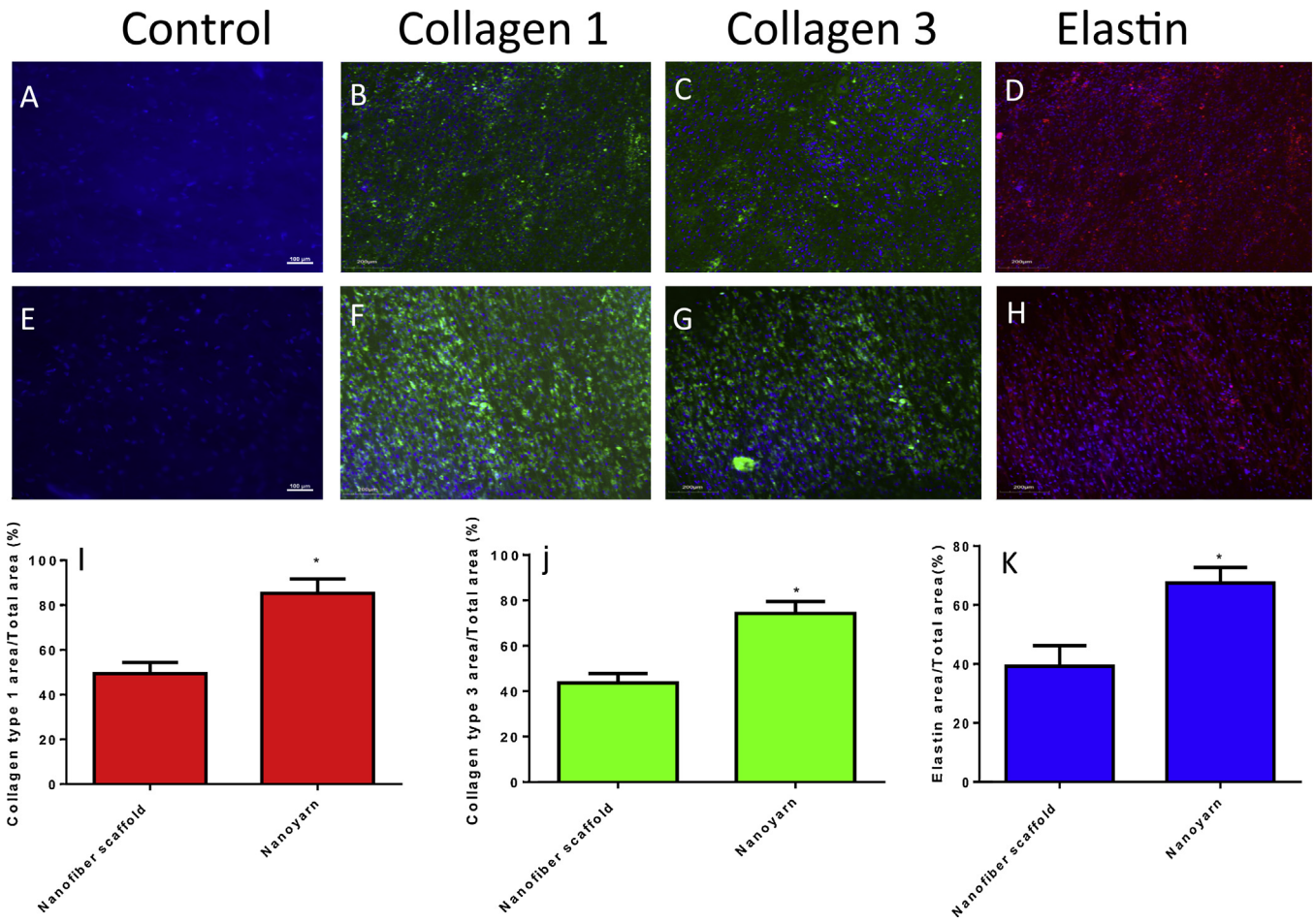

Fig. 8. The immunofluorescence of ECM. Nanofiber scaffold immunostained for collagen type 1 (B), collagen type 3 (C) and elastin (D). Nanoyarn scaffold immunostained for collagen type 1 (F), collagen type 3 (G) and elastin (H). The cell-seeded nanofiber scaffold (A) and nanoyarn (B) stained without primary antibodies were as control. The quantitative analysis of the density for the collagen type 1 (I), collagen type 3 (J) and elastin (K), *$p < 0.05$, $n = 5$.

showed aligned actin filaments which means that the myoblasts sensed the substrates topography and transform such information into morphological changes, then exhibited native morphology on the nanoyarn scaffolds. The histology image (Fig. 7) showed higher cells infiltration in the nanoyarn scaffolds. After migrating into the nanoyarn, the myoblasts exhibited a 3D culture pattern, with more space for proliferation. However, the nanofiber scaffold limited the space for cell proliferation.

Surface topography of the scaffolds plays major role in regulating cell gene expression. According to the collagen assay, there was more production of total collagen in the myoblasts seeded nanoyarn compared with nanofiber scaffolds and 2D culture (Supplementary Fig. 2). In the present study, we focused on evaluating the expression of ECM with immunofluoresence and analyzing it semi-quantitatively. In ECM, collagen type 1, type 3 and elastin are the primary matrix components of muscle tissue [30]. Large amount of the collagen type 1, collagen type 3 and elastin were deposited densely along the aligned yarn, however, they were distributed at the surface of nanofiber scaffold randomly and loosely (Fig. 8). The ECM and muscle specific genes expression at the mRNA level was determined through real-time PCR (Supplementary Fig. 3). At day 7, the collagen type 1 and collagen type 3 expression levels of myoblasts on nanoyarn were higher than those on the nanofiber scaffolds. The genes of muscle specific markers, α-actin and desmin, were elevated in nanoyarn which suggested that a higher potential for myoblasts-nanoyarn construct to be developed into the muscle tissue. In our study, the blended collagen and P(LLA-CL) solution ratio is 50:50, it could not only highly improve the cells proliferation but also maintain a good mechanical property. This ratio of collagen to P(LLA-CL) could be a promising fomula of biomaterial for tissue engineered sling.

The contraction rate of the scaffolds without and with cells were examined. We found a significantly high contraction rate in nanofiber scaffolds seeded with cells compared with nanoyarn scaffolds. This low contraction property of nanoyarn is important for clinical use and does not change the original mechanical properties after it was fixed to the right position. Although the nanoyarn still exhibited contraction to a certain extent, it could be prevented *in vitro* by restraint technique [31].

The nanoyarn showed a lower Young's modulus, lower tensile strength but higher elongation at break compared with nanofiber scaffold. After the myoblasts seeding and 7 day's culture, the nanoyarn scaffold revealed an elevation of Young's modulus and tensile strength significantly. However, the elevation of mechanical properties in nanofiber scaffold was not significant after cell seeding. These results demonstrated that the cells had a better proliferation in nanoyarn scaffold and more ECM deposition in 7 days' time, which increased the thickness and strength of the nanoyarn. The larger pores and higher porosity reduced the tensile strength and young's modulus of nanoyarn to some extent but increased the elastisity. This property is also possessed in the commercialized slings and gracilis muscle sling [32,33]. The SIS and PLA are two recomended material as the candidates for engineered sling in a paper comparing 7 different materials for tissue engineered sling,

but the Young's modulus of them are also lower than native tissue (6–8 MPa) [31]. However, the tensile strength of our nanoyarn could surpass that of native tissue (1 MPa) [31]. Thus, despite of the advantage of cell proliferation, cell infiltration and gene expression of nanoyarn, the mechanical property should be one of the point needed to be reformed to mimic the native tissue.

The function of nanoyarn for increasing expression of the collagen and muscle specific markers has never been studied before. In the present study, we systematically evaluated the compatibility of novel scaffold to the myoblasts, including the myoblasts infiltration and tissue development with F-actin staining, ECM immunofluorescence and real-time PCR to assess the functional expression. The study provided a more stable foundation for the future research of this material for *in vivo* study compared with the previous researches. The limitation of the present study is that we compared the nanoyarn with the random nanofiber scaffold, because it is not feasible to seed the commercialized sling with cells. The novel nanoyarn will be compared with an aligned nanofiber scaffold and some commercialized slings in the *in vivo* study.

Although the positive influence of aligned and porous scaffold is well known, however, previous studies in the field of tissue engineering and biomaterials did less mechanism study of the interaction between cells and scaffolds. One of the causes might be the cell lines they used are from small animals which are lack of gene chips to do the high throughput screening. Our present study observed the phenomenon of the human placental stem cells' behavior in an aligned, large-pore scaffold. In the next step, we will evaluate the change of molecules in some popular signaling pathways like TGF-β, Wnt, Notch and micro-RNAs as well which played important roles in cell development and the ECM production to discover the mechanism of cell-scaffold interaction.

In the process of nanoyarn fabrication, the vortex is important for twisting the fibers together. The spinning speed of the vortex might be influenced by the volume of water in the basin and the size of the hole. However, at present, we only possess one dynamic liquid system in our lab, so, the parameters of fabrication were relatively constant. The study about the morphology and function of nanoyarn at different conditions could be done in the future.

5. Conclusion

PSCs could be induced to myoblasts and revealed higher muscular cell markers and ECM expression. These myoblasts could become a potential cell source for tissue engineered sling. Furthermore, a novel electrospun nanoyarn was fabricated with dynamic liquid electrospinning. The *in vitro* study demonstrated that the nanoyarn could improve myoblasts proliferation, muscle development and ECM expression compared with nanofiber scaffold. The cooperation of myoblasts and nanoyarn scaffold could be a promising tissue engineered sling for our *in vivo* study in the future.

Conflict of interest

There is no conflict of interest among the authors.

Acknowledgements

It is very much appreciated that the contribution has been made by the Biomaterials and Tissue Engineering Laboratory, College of Chemistry &Chemical Engineering and Biotechnology, Donghua University in the work of fabrication of scaffold. It is also very much appreciated that Wake Forest Institute for regenerative medicine, Winston-Salem, North Carolina, USA made a lot of contributions to this study. The study was supported by Science and Technology Commission of Shanghai Municipality (14JC1492100).

Appendix A. Supplementary data

Supplementary data associated with this article can be found, in the online version, at http://dx.doi.org/10.1016/j.colsurfb.2016.03.083.

References

[1] P. Norton, L. Brubaker, Urinary incontinence in women, Lancet 367 (2006) 57–67.
[2] M.Y. Kim, S.D. Choi, A. Ryu, Is complementary and alternative therapy effective for women in the climacteric period? J. Menopausal Med. 21 (2015) 28–35.
[3] L.S. MacLachlan, E.S. Rovner, New treatments for incontinence, Adv. Chronic Kidney Dis. 22 (2015) 279–288.
[4] C. Tran, M.S. Damaser, The potential role of stem cells in the treatment of urinary incontinence, BioMed Res. Int. 7 (2015) 22–40.
[5] X.H. Zou, Y.L. Zhi, X. Chen, et al., Mesenchymal stem cell seeded knitted silk sling for the treatment of stress urinary incontinence, Biomaterials 31 (2010) 4872–4879.
[6] D. Kwon, Y. Kim, R. Pruchnic, et al., Periurethral cellular injection: comparison of muscle-derived progenitor cells and fibroblasts with regard to efficacy and tissue contractility in an animal model of stress urinary incontinence, Urology 68 (2006) 449–454.
[7] S. Roman, A. Mangera, N.I. Osman, A.J. Bullock, C.R. Chapple, S. MacNeil, Developing a tissue engineered repair material for treatment of stress urinary incontinence and pelvic organ prolapse-which cell source? Neurourol. Urodyn. 33 (2014) 531–537.
[8] M.S. Oliveira, J.B. Barreto-Filho, Placental-derived stem cells: culture, differentiation and challenges, World J. Stem Cells. 7 (2015) 769–775.
[9] S. Gennai, A. Monsel, Q. Hao, et al., Cell-based therapy for traumatic brain injury, Br. J. Anaesth. 115 (2015) 203–212.
[10] X.Wang, J. Zhang, F. Zhang et al. The clinical status of stem cell Therapy for ischemic cardiomyopathy. 2015: 135023.
[11] S.V. Murphy, A. Atala, Amniotic fluid and placental membranes: unexpected sources of highly multipotent cells, Semin. Reprod. Med. 31 (2013) 62–68.
[12] R. Mahmood, M.S. Choudhery, A. Mehmood, S.N. Khan, S. Riazuddin, In vitro differentiation potential of human placenta derived cells into skin cells, Stem Cells Int. 2015 (2015) 841062.
[13] J.C. Bridge, J.W. Aylott, C.E. Brightling, et al., Adapting the electrospinning process to provide three unique environments for a tri-layered In vitro model of the airway wall, J. Vis. Exp.: JoVE. (2016) 2015.
[14] C. Liu, C. Zhu, J. Li, et al., The effect of the fibre orientation of electrospun scaffolds on the matrix production of rabbit annulus fibrosus-derived stem cells, Bone Res. 3 (2015) 15012.
[15] J.T. Martin, A.H. Milby, K. Ikuta, et al., A radiopaque electrospun scaffold for engineering fibrous musculoskeletal tissues: scaffold characterization and in vivo applications, Acta Biomater. (2015).
[16] J. Wu, C. Huang, W. Liu, et al., Cell infiltration and vascularization in porous nanoyarn scaffolds prepared by dynamic liquid electrospinning, J. Biomed. Nanotechnol. 10 (2014) 603–614.
[17] Q. Fu, X.F. Song, G.L. Liao, C.L. Deng, L. Cui, Myoblasts differentiated from adipose-derived stem cells to treat stress urinary incontinence, Urology 75 (2010) 718–723.
[18] A.M. Kajbafzadeh, S. Mozafarpour, S.S. Ladi Seyedian, R. Khorramirouz, H. Nasser Hojjati, Decellularized dermal strip as a suburethral sling in a rat model of stress urinary incontinence, Int. Urol. Nephrol. 47 (2015) 1303–1310.
[19] L. Hakim, D. De Ridder, F. Van der Aa, Slings for urinary incontinence and the application of cell-based therapy, Adv. Drug Deliv. Rev. 82–83 (2015) 22–30.
[20] C.P. Barnes, S.A. Sell, E.D. Boland, D.G. Simpson, G.L. Bowlin, Nanofiber technology: designing the next generation of tissue engineering scaffolds, Adv. Drug Deliv. Rev. 59 (2007) 1413–1433.
[21] Z. Guo, J. Xu, S. Ding, H. Li, C. Zhou, L. Li, In vitro evaluation of random and aligned polycaprolactone/gelatin fibers via eletrospinning for bone tissue engineering, J. Biomater. Sci. Polym. Ed. 2015 (2016) 1–26.
[22] I. Ortega, L. Dew, A.G. Kelly, C.K. Chong, S. MacNeil, F. Claeyssens, Fabrication of biodegradable synthetic perfusable vascular networks via a combination of electrospinning and robocasting, Biomater. Sci. 3 (2015) 592–596.
[23] S. Sridhar, J.R. Venugopal, R. Sridhar, S. Ramakrishna, Cardiogenic differentiation of mesenchymal stem cells with gold nanoparticle loaded functionalized nanofibers, Coll. Surf. B, Biointerfaces 134 (2015) 346–354.
[24] S. Khorshidi, A. Solouk, H. Mirzadeh, et al., A review of key challenges of electrospun scaffolds for tissue-engineering applications, J. Tissue Eng. Regen. Med. (2015).
[25] B.M. Baker, A.M. Handorf, L.C. Ionescu, W.J. Li, R.L. Mauck, New directions in nanofibrous scaffolds for soft tissue engineering and regeneration, Expert Rev. Med. Devices 6 (2009) 515–532.
[26] C. Yang, G. Deng, W. Chen, X. Ye, X. Mo, A novel electrospun-aligned nanoyarn-reinforced nanofibrous scaffold for tendon tissue engineering, Coll. Surf. B, Biointerfaces 122 (2014) 270–276.
[27] S.B. Orr, A. Chainani, K.J. Hippensteel, et al., Aligned multilayered electrospun scaffolds for rotator cuff tendon tissue engineering, Acta Biomater. 24 (2015) 117–126.

[28] D. Li, T. Wu, N. He, et al., Three-dimensional polycaprolactone scaffold via needleless electrospinning promotes cell proliferation and infiltration, Coll. Surf. B, Biointerfaces 121 (2014) 432–443.
[29] V. Beachley, X. Wen, Polymer nanofibrous structures: fabrication, biofunctionalization, and cell interactions, Prog. Polym. Sci. 35 (2010) 868–892.
[30] P. Chandra, S.J. Lee, Synthetic extracellular microenvironment for modulating stem cell behaviors, Biomark. Insights 10 (2015) 105–116.
[31] A. Mangera, A.J. Bullock, S. Roman, C.R. Chapple, S. MacNeil, Comparison of candidate scaffolds for tissue engineering for stress urinary incontinence and pelvic organ prolapse repair, BJU Int. 112 (2013) 674–685.
[32] J.G. Blaivas, R.S. Purohit, M.S. Benedon, et al., Safety considerations for synthetic sling surgery, Nat. Rev. Urol. (2015).
[33] M.D. Gershbaum, J.A. Stock, M.K. Hanna, Gracilis muscle sling for select incontinent bladder exstrophy cripples, J. Urol. 165 (2001) 2422–2424.